# SNS LOW-LEVEL RF CONTROL SYSTEM: DESIGN AND PERFORMANCE *

Hengjie Ma, Mark Champion, Mark Crofford, Kay-Uwe Kasemir, Maurice Piller,
Oak Ridge National Laboratory, Oak Ridge , TN37831, U.S.A
Lawrence Doolittle, Alex Rotti, LBNL, Berkeley, California, U.S.A.

*Abstract*

A full digital RF field control module (FCM) has been developed for SNS LINAC. The digital hardware for all the control and DSP functionalities, including the final vector modulation as well as IF output synthesis, is implemented on a single high-density FPGA. Two of its HDL models have been written in VHDL and Verilog respectively, and both have being used to support the testing and commissioning of the LINAC to the date. The control algorithm used in the HDL produces a latency as low as 150nS. During the commissioning, the flexibility and capacity for needed precise controls that only digital design can provide has proved to be a necessity for meeting the great challenge of a high-power pulsed SCL.

## SYSTEM DESCRIPTION

The basic design of SNS digital LLRF feedback control system is a straightforward digital implementation of a series P-I controller in a textbook configuration. The description of the RF control system may start with a familiar state variable representation of a RLC equivalent circuit model for a typical cavity, as well the transfer function of the P-I controller as the following ;

$$\frac{d\boldsymbol{v}_p(t)}{dt} = \boldsymbol{A}\cdot\boldsymbol{v}_p(t) + \omega_b \cdot R_L \cdot \boldsymbol{i}_g(t) \tag{1a}$$

$$\boldsymbol{i}_g(t) = \boldsymbol{g}\cdot\boldsymbol{K}_p\cdot[(\boldsymbol{e}(t) + K_I\int_{t0}^{t1}\boldsymbol{e}(t)\cdot dt] \tag{1b}$$

$$\boldsymbol{e}(t) = \boldsymbol{v}_p(t) - \boldsymbol{V}_S$$

where $v_p(t)$, $\boldsymbol{A}$ and $\omega_b$ are , as usual, the complex phasor of cavity probe voltage, the state transition matrix, and the half bandwidth of the cavity respectively. Quantity $\boldsymbol{i}_g(t)$ is the input current drive to the cavity, and $\boldsymbol{g}$ is the trans-admittance which represents a lumped-effects of high-power amplifiers, signal transmission, as well as the impedance-matching devices. Quantity $\boldsymbol{Vs}$ is

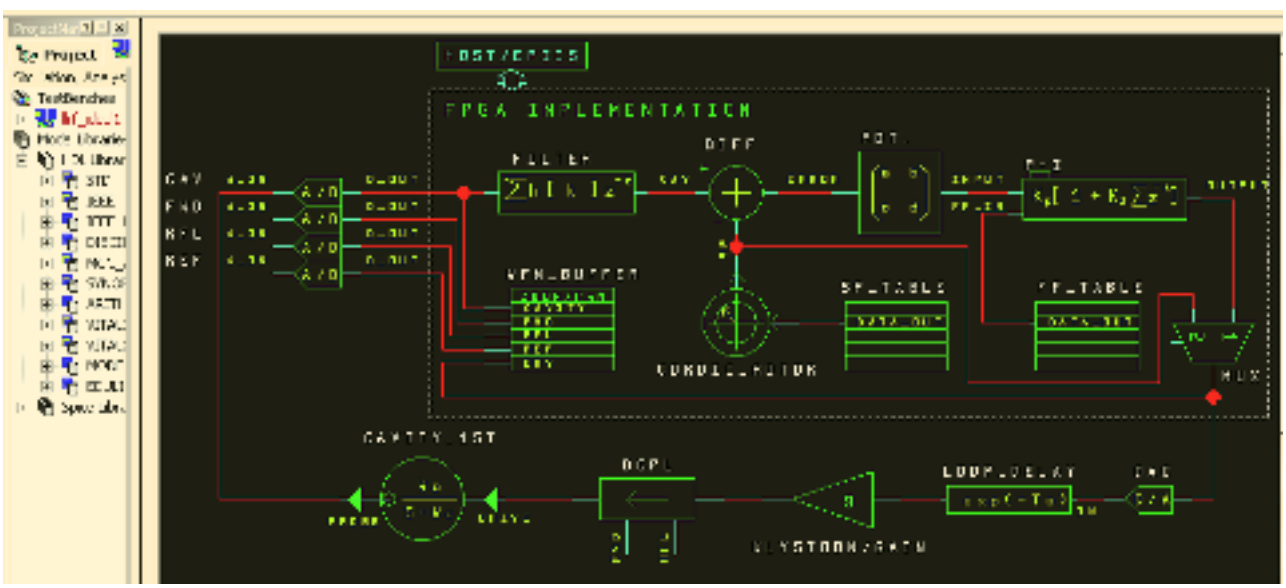


Figure 1: Mixed-signal model of SNS LLRF system.

the set point for the field. The integral term is included as it may be necessary for achieving the specified field regulation error of 1% or less. The details about P-I controller as well as the cavity modeling can be found in many publications[1],[2],[3],[4]. Using a direct 1st-order approximation in the discrete-time domain for the derivative and integral term in (1a) and (1b), we can express the transfer function $G_c(z)$ for a P-I controller algorithm in z-domain as

*SNS is managed by UT-Battelle, LLC, under contract DE-AC05-00OR22725 for the U.S. Department of Energy. SNS is a partnership of six national laboratories: Argonne, Brookhaven, Jefferson, Lawrence Berkeley, Los Alamos and Oak Ridge



0-7803-8859-3/05/$20.00 ©2005 IEEE

$$G_c(z) = \omega_b \cdot R_L \cdot \boldsymbol{K_p} \cdot [1 + T_s \cdot K_i \sum_{k=0}^{n} z^{-k}] \quad (1c)$$

which suggests a straightforward implementation. We can also obtain the cavity model $G_p(z)$ as

$$G_p(z) = z^{-M} \cdot \frac{(1 - e^{-\tau \cdot \omega_b})z - 1}{1 - e^{-\tau \cdot \omega_b} z - 1} \quad (1d)$$

where $M = floor(\tau / T_s)$, $\tau$ is loop delay and $T_s$ is the time interval of sampling. The plant model $G_p(z)$ is needed later on for determining an optimized algorithm other than the textbook form in (1c). With the mixed-signal modeling capability of VHDL-ASM, the behavior of the digital controller and the analog components in the rest of the RF system can be modeled and analyzed together in one HDL. Figure 1 is a symbolic representation of such a mixed-signal model. In the digital implementation, beside the required P-I algorithm, there are also a few added supporting functionalities necessary for system operation. Those functionalities include five data buffers of 1k-word each for recording the signal waveforms, and two parameter tables for the set-point curve and feed-forward waveforms. A CORDIC algorithm based phasor rotator is also coded in the HDL . The rotator spins the set-point phasor to shift the output frequency up to +/-645kHz when needed during cavity tuning and heating. After PAR on FPGA chip XC2V1500, the entire design has taken about 20% of logic slices, 20% of RAMBs, 50% of IOBs, and 8% of multipliers on the chip, leaving more than 50% chip resources for future expansion. The control algorithm allows the signal data to pass through the controller in 6 clock cycles (150 nS).

## PERFORMANCE AND TUNING

The system analysis at the cavity probe where the end-to-end point is defined can be conveniently carried out in continuous-time. For simplification, we are omitting the Lorentz force related effects. The equation (1a) and (1b) therefore describe a LTI system, and their Laplace solution gives the system open-loop transfer function as

$$\begin{aligned} G(s) &= \boldsymbol{K_p} \cdot (1 + \frac{K_i}{s}) \cdot \frac{\omega_b}{s + \omega_b} \cdot e^{-\tau \cdot s} \cdot \boldsymbol{g} \\ &= \boldsymbol{g} \cdot \boldsymbol{K_p} \cdot \frac{\omega_b (s + K_i)}{s(s + \omega_b)} \cdot e^{-\tau \cdot s} \end{aligned} \quad (2a)$$

For an unity feedback, the closed-loop transfer function is

$$G_B(s) = \frac{G(s)}{1 + G(s)} = \frac{\boldsymbol{g} \cdot \boldsymbol{K_p} \cdot \omega_b (s + K_i) \cdot e^{-\tau \cdot s}}{s(s + \omega_b) + \boldsymbol{g} \cdot \boldsymbol{K_p} \cdot \omega_b (s + K_i) \cdot e^{-\tau \cdot s}} \quad (2b)$$

which indicates a Type 1, $n_{th}$-order system.

### *Limiting Effect of Loop Delay*

The added poles due to the loop delay $\tau$ has created the possibility for instability to occur, and limited the maximum loop gain that can be used , and that in turn limited the control bandwidth and precision. To illustrate

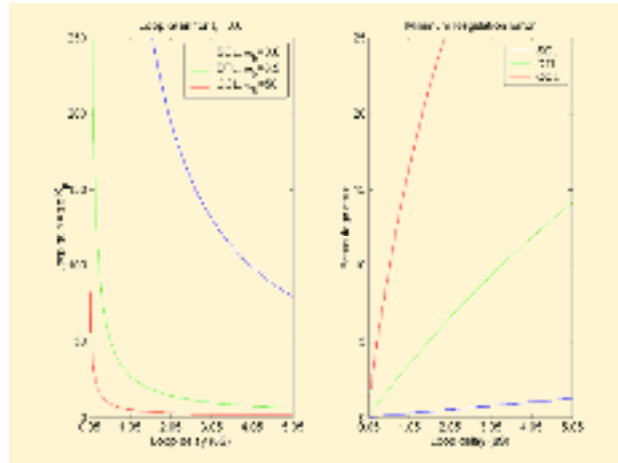

Figure 2: Case of proportional control only.

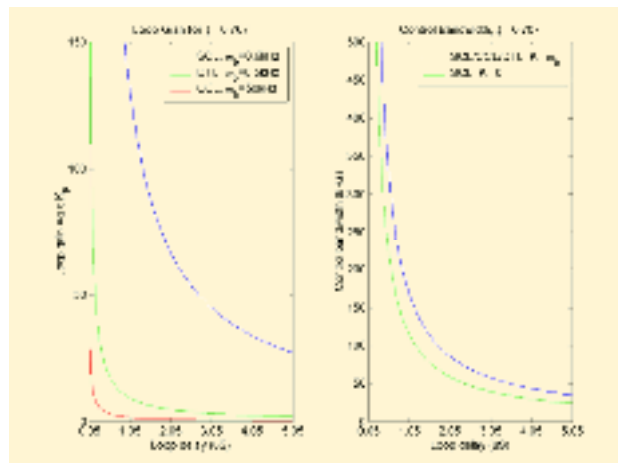

Figure 3: Effect of loop delay on loop gain and control bandwidth, case of P-I control.

this point, let's first study two cases;

Case 1. Simplest proportional controller. In this case, we set $K_i$ =0 in (2b). Substituting the exponential term for the delay with a Pade approximation of n=1 and m=2, and assuming a real loop gain, we obtain the characteristic equation F(s) for the closed-loop system as

$$F(s) = \left(1 + \frac{\tau \cdot K}{6}\right) s^2 + \left(1 + \frac{\tau \cdot \omega_b}{3} - \frac{2\tau \cdot K}{3}\right) s + (\tau \cdot \omega_b + \tau \cdot K) = 0 \quad (2c)$$

where $K = g \cdot K_p \cdot \omega_b$. By Routh-Hurwitz criterion for control stability, the maximum total loop allowed in this Type 0 2nd-order system and smallest control error possible under the gain constraint are plotted in Figure 2. From the plots we can see that with the typical 1uS loop delay that SNS system has, the design specification of 1% in the error cannot be met with the proportional control only configuration for DTL and CCL. However, for SCL, the use of this configuration may still be possible.

Case 2. P-I control with Ki = $\omega_b$. Here we are tuning the system by matching the time constant of controller to that

of the cavity. The cavity pole is therefore cancelled, and

$$G(s) = \boldsymbol{K_p} \cdot (1 + \frac{K_i}{s}) \cdot \frac{\omega_b}{s + \omega_b} \cdot e^{-\tau \cdot s} \cdot \boldsymbol{g}$$
$$= \boldsymbol{g} \cdot \boldsymbol{K_p} \cdot \frac{\omega_b}{s} \cdot e^{-\tau \cdot s} \quad (2d)$$

Again using a Pade approximation and Routh-Hurwitz criterion, we obtain a Type 1, 2nd-order system with a characteristic equation F(s) as

$$F(s) = s(1 + \frac{1}{3}\tau s) + \boldsymbol{g} \cdot \boldsymbol{K_p} \cdot \omega_b \left(1 - \frac{2}{3}\tau s + \frac{1}{6}(\tau s)^2\right) = 0 \quad (2e)$$

and the maximum value of gain-bandwidth product $g \cdot K_p \cdot \omega_b$. The maximum loop gain and step function response time Ts are plotted as a function of delay τ and cavity bandwidth in **Figure 3.** The case for $K_i$=0 is also plotted in this figure for comparison.

### *Test Results*

All LLRF systems in the warm section of SNS LINAC are tuned up with the method of integral zero-cavity pole cancellation. The result for DTL-1 in **Figure 4** shows the system time response to a 12.5% step function change in the field set value. With the cavity bandwidth of 8.5kHz, the 4.3 uS for 95% settling time and 110kHz control bandwidth are close to the predicted performance. Along the excellent time response, there is a glaring overshoot in the drive power which indicates the typical behavior of a dead-beat controller. A constraint for the power overshoot can be easily added once an acceptable compromise in the performance is decided.

All the analysis we have done so far is based on an assumption of having a linear time-invariant system. This assumption is no longer valid on SCL cavities due to the effect of Lorentz detuning and limited Klystron power margin. **Figure 5** is a test result on a SCL cavity running at relative low field gradient. The actual loop gain that could be applied for proportional control only was limited to only 20 which is far less than the predicated value for critical damping, resulting in a stable operation but with 5% steady-state error. When the integral control was added, the error was removed, but

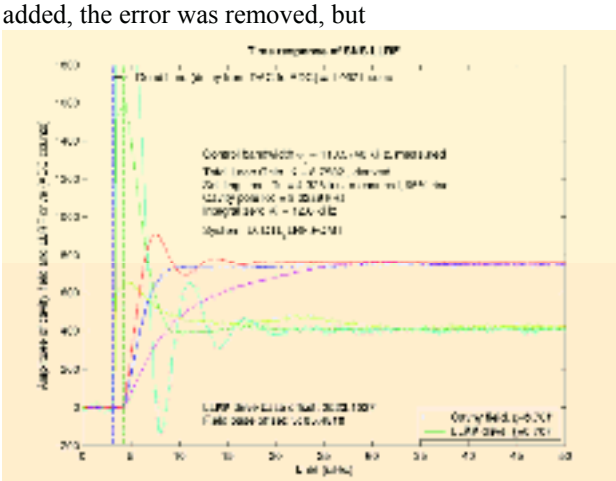

Figure 4: System response on DTL-1 under optimal.

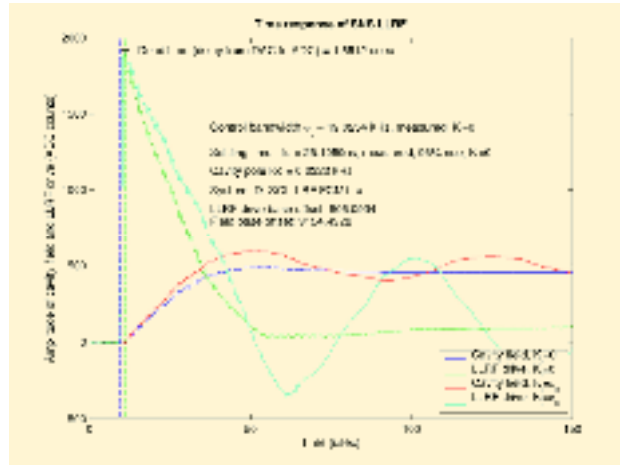

Figure 4: Response of a SCL under an extremely over-damped control.

induced an oscillation of about 15kHz in the system. The reason that caused this resonance is unclear at this time. But it seemed there is a possibility of mechanical-electrical coupling facilitated by Lorentz force on the cavity, as well as the phase condition by the integral term.

## DISCUSSION

The high power pulsed supper-conducting LINAC presents a great challenge to LLRF controls. The interaction between Lorentz detuning and the LLRF controls needs to be understood. The digital implementation on large FPGA chips provides the capability and flexibility which allows a continuing R&D for more sophisticated control techniques. The newer VHDL-AMS can be a great tool for this R&D effort for its capability of performing integrated end-to-end system simulations and verifications not only across the signal-domains, but also across the physical-domains

## ACKNOWLEDGEMENT

The authors would like to extend their sincere appreciation to Craig Swanson of Alpha CAD, as well as Matt Stettler and John Power of LANL for their important contribution in the development of FCM under a difficult circumstance.

## REFERENCES

[1] B. C. Kuo, "Automated Control systems," Prentice-Hall, 1987.

[2] T. Czarski, et. al, "Cavity control system essential modeling for TESLA linear accelerator," TESLA Report 2003-08.

[3] L. Doolittle, "Low Level RF Modeling for the MEBT Rebunchers," LBNL SNS Tech Note FE-EE-021, FE3000, June 13, 2001.

[4] L. Doolittle, "Plan for a 50MHz Analog Output Channel," LBNL posted tech note, August 8, 2002.



0-7803-8859-3/05/$20.00 ©2005 IEEE